



## A truncated conical beam model for analysis of the vibration of rat whiskers



Wenyi Yan<sup>a,\*</sup>, Qianhua Kan<sup>b</sup>, Kenan Kergrene<sup>c</sup>, Guozheng Kang<sup>b</sup>,  
Xi-Qiao Feng<sup>d</sup>, Ramesh Rajan<sup>e</sup>

<sup>a</sup> Department of Mechanical & Aerospace Engineering, Monash University, Wellington Road, Clayton, VIC 3800, Australia

<sup>b</sup> School of Mechanics and Engineering, Southwest Jiaotong University, Chengdu 610031, China

<sup>c</sup> Département de Génie Mécanique, Ecole Normale Supérieure de Cachan, France

<sup>d</sup> Department of Engineering Mechanics, Tsinghua University, Beijing 100084, China

<sup>e</sup> Department of Physiology, Monash University, Clayton, VIC 3800, Australia

### ARTICLE INFO

#### Article history:

Accepted 13 June 2013

#### Keywords:

Rat whisker  
Vibrissa mechanics  
Truncated conical beam  
Vibration  
Natural frequency

### ABSTRACT

A truncated conical beam model is developed to study the vibration behaviour of a rat whisker. Translational and rotational springs are introduced to better represent the constraint conditions at the base of the whiskers in a living rat. Dimensional analysis shows that the natural frequency of a truncated conical beam with generic spring constraints at its ends is inversely proportional to the square root of the mass density. Under all the combinations of the classical free, pinned, sliding or fixed boundary conditions of a truncated conical beam, it is proved that the natural frequency can be expressed as  $f = \alpha(r_b/L^2)\sqrt{E/\rho}$  and the frequency coefficient  $\alpha$  only depends on the ratio of the radii at the two ends of the beam. The natural frequencies of a representative rat whisker are predicted for two typical situations: freely whisking in air and the tip touching an object. Our numerical results show that there exists a window where the natural frequencies of a rat whisker are very sensitive to the change of the rotational constraint at the base. This finding is also confirmed by the numerical results of 18 whiskers with their data available from literature. It can be concluded that the natural frequencies of a rat whisker can be adjusted within a wide range through manipulating the constraints of the follicle on the rat base by a behaving animal.

© 2013 Elsevier Ltd. All rights reserved.

### 1. Introduction

Rats, a ubiquitous and highly successful mammalian species that carry out most of their activities in nocturnal poor-light conditions, use their smell and their large face whiskers (macro-vibrissae or vibrissae for short) to perceive the world. A Chinese idiom says that “the eyes of a rat can see only an inch of light”, which vividly describes rat's poor sight. During a typical exploration, rats sweep the large face whiskers against and over an object to obtain information such as its position, shape and surface properties, and identity (Jadhav and Feldman, 2010). Using even just a single whisker, a blindfolded rat can discriminate between smooth and fine grooved surfaces with groove depth of 30  $\mu\text{m}$  and groove spacing interval of 90  $\mu\text{m}$  (Carvell and Simons, 1990), while another study showed that rats can use their whiskers to discriminate between apertures of 62 and 68 mm width (Krupa et al., 2001).

Information is gained from the deflection of their whiskers either passively as the rat brushes past an object, or actively when rats “whisk” their facial vibrissae under muscle control, to sweep forwards and backwards against and over an object. Mechanical interactions between the moving whiskers and objects can cause whisker vibration or even resonance which multiplies motion amplitude at the whisker's fundamental resonance frequency (Hartmann et al., 2003; Neimark et al., 2003; Andermann et al., 2004; Ritt et al., 2008) and significantly lowers the threshold for evoked neural activity in the rat's cortex (Andermann and Moore, 2008). The whiskers vary systematically in length and thickness across the face (long and thin at the back, short and stubby at the front) and in turn whisker fundamental frequency varies systematically with whisker position across the face, allowing for encoding of a range of different textures. The whisker resonance theory is considered as one of three existing theories to explain how a rat discriminates surface texture, i.e., to distinguish a rough surface from a smooth surface (Jadhav and Feldman, 2010). Therefore, to study whisker resonance and their natural frequencies can assist the understanding of this exquisite tactile sensory system.

There are no receptors along the length of the whisker and therefore all tactile information must be mechanically transmitted

\* Corresponding author. Tel.: +61 3 99020113; fax: +61 3 99051825.  
E-mail address: [wenyi.yan@monash.edu](mailto:wenyi.yan@monash.edu) (W. Yan).

back to receptors at the whisker base (Ebara et al., 2002; Rice et al., 1997). From the mechanics viewpoint, a sweeping rat whisker can be treated as a dynamic beam and, in fact, the engineering beam theory has been applied to understand the mechanical behaviour of rat whiskers. For example, Hartmann et al. (2003) studied the whisker vibration by imposing a sinusoid displacement at the base of a whisker glued to a vibration table and then, in their theoretical analysis, treated the whisker as a truncated conical beam with free tip and fixed base boundary conditions. Assuming that all the 24 studied rat whiskers have the same elastic modulus, they found that the elastic modulus of the rat whiskers is in the range of 3–4 GPa (Hartmann et al. 2003). A fully conical beam model was applied by Neimark et al. (2003) to interpret their *in vivo* and *ex vivo* experiments on rat whiskers. They have analysed a total of 18 whiskers across the face, including their geometrical data, mass and first natural frequencies under *in vivo* fixed-tip condition.

Transverse vibration of geometrically non-uniform beams is a classic problem in vibration mechanics. The earliest study was carried out by Kirchhoff in 19th century (Sanger, 1967; Weaver et al., 1990). Conway and Dubil (1965) presented tables of numerical values of natural frequencies of truncated conical beam and wedges for all the combinations of boundary conditions, namely the conventional free, simply supported (pinned) and fixed boundary condition. Sanger (1967) extended the problem to beams with a more general variation in cross-section under conventional boundary conditions. Prismatic beams with elastic supports represented by spring elements at the beam ends were discussed in Weaver et al. (1990).

The objective of current study is to theoretically re-examine the vibration problem of rat whiskers with emphasis on the analysis of natural vibration frequencies. Experimental measurements show that the tip of rat whisker is not ideally sharp (e.g., Quist et al., 2011). Additionally, as observed in awake, behaving animals, the whisker may bump into an object, stick against it and then whisk past it (Hartmann et al. 2003)—the so-called “stick-slip” behaviour that is also postulated to play a role in texture discrimination (Wolfe et al., 2008; Ritt et al., 2008). Therefore, a truncated cone is applied to simulate the geometry of rat whiskers. Considering that the base of the rat whisker is attached underneath the skin in a follicle–sinus complex (Ebara et al., 2002) in an animal, a more realistic constraint of a transverse and a rotational spring is applied in our model to simulate such an elastic body support at the base. To cover all real situations for the rat whisker tip, similar constraints are applied to the tip in our model.

## 2. Truncated conical model

The rat whisker is a thin, long, pliable hair, attached underneath the skin in a follicle–sinus complex (FSC), (Ebara et al., 2002; and see Fig. 1(a)). From a structural mechanics viewpoint, the whisker can be modelled as a Bernoulli–Euler beam. The radii of the whiskers measured at different locations by Neimark et al. (2003) and Voges et al. (2010) indicate that the whisker can be described as conical in shape; hence, as illustrated in Fig. 1(b), a truncated cone is used to describe the geometry of a rat whisker.  $L$  and  $L_2$  are the length of the truncated and “chopped” (absent) cones, respectively.  $L_1$  represents the length of the original full cone.  $r_t$  and  $r_b$  are respectively the radius at the tip and the base of the rat whisker. The radius of the beam cross-section evolves linearly along the axial direction, i.e., the  $x$ -direction. It is worth noting that the rat whisker in our current theoretical study is treated as a straight beam. In reality, some whiskers, especially the very long caudal whiskers, are curved in shape. The effect of the initial curvature is not considered in our current study. Additionally, we limit our study to free vibration without damping, a parameter that may affect the resonant

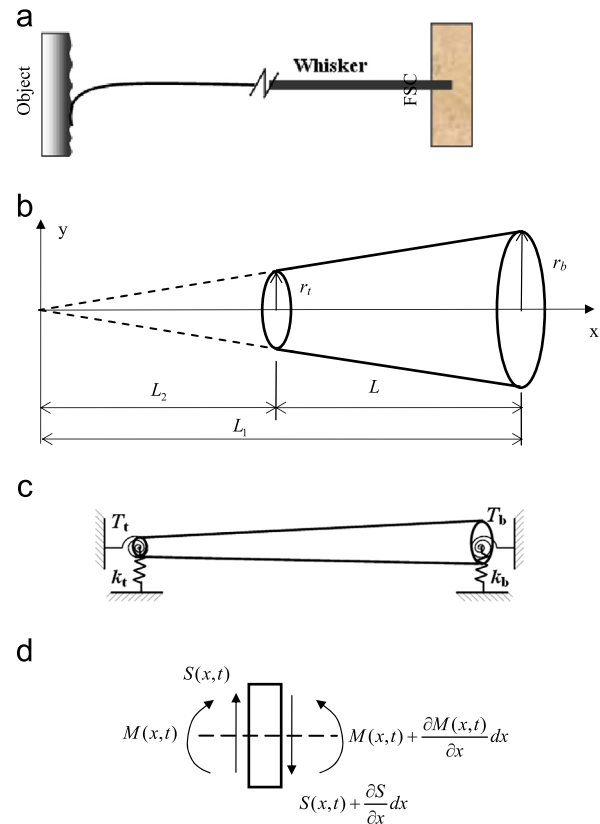


**Fig. 1.** (a) Illustration of a rat whisker sweeping an object; (b) a truncated cone for modelling rat whiskers with specified geometrical parameters (not to scale); (c) schematic of a torsional–torsional boundary condition for the truncated beam model to simulate *ex vivo* or *in vivo* rat whisker vibration; and (d) infinitesimal beam element for establishing the differential equation.

frequencies. Both initial curvature and damping will be considered in our future studies.

Given that the boundary condition at the whisker base cannot be really considered fixed or pinned due to facial compliance in the follicle (Hartmann et al., 2003), the elastic constraints in both transverse and angular directions are more realistic. Similarly, the rat whisker tip may vibrate freely in air or touch a soft/hard object. Generically, all possible boundary conditions at the two ends of the whisker can be represented by spring elements with translational springs to constrain the transverse deflection and rotational springs to constrain the angular movement. Considering linear constraints,  $k_t$  and  $T_t$  are the stiffness constants for the translational and rotational springs at the whisker tip, and  $k_b$  and  $T_b$  are the stiffness constants at the whisker base (see Fig. 1c). The classical free, pinned, sliding and fixed conditions can be considered as special cases from this generic treatment.

For transverse free vibration, the forces and moments applied on an infinitesimal element at arbitrary location  $x$  are illustrated in Fig. 1(d). Under the assumption of small deformation and small rotation for a Bernoulli–Euler beam, applying the dynamic equilibrium condition for the forces and the moment equilibrium equation, the following partial differential equation can be obtained:

$$\frac{\partial^2}{\partial x^2} \left[ EI(x) \frac{\partial^2 v(x,t)}{\partial x^2} \right] + \rho A(x) \frac{\partial^2 v(x,t)}{\partial t^2} = 0 \quad (1)$$

where  $I(x)$  and  $A(x)$  are the moment of inertia and the cross-section area at location  $x$ , respectively.  $v(x,t)$  is the transverse displacement.  $E$  and  $\rho$  are the elastic modulus and mass density of the rat whisker material, respectively. Here, the rat whisker material is assumed as

isotropic and homogenous. When the rat whisker vibrates transversely in one of its natural modes  $n$ , the transverse displacement at any location  $v(x, t)$  varies harmonically with time (Weaver et al., 1990), i.e.,

$$v(x, t) = y(x) \sin(\omega_n t + \phi) \tag{2}$$

where  $\omega_n$  is the circular (angular) frequency for the natural mode  $n$ . (Without causing any confusion, the subscript  $n$  is neglected hereafter.)

The natural frequency  $f$  is related to its circular frequency  $\omega$  by

$$f = \frac{\omega}{2\pi} \tag{3}$$

Substituting Eq. (2) into Eq. (1) results in

$$\frac{d^2}{dx^2} \left( EI(x) \frac{d^2 y(x)}{dx^2} \right) - \rho A(x) \omega^2 y(x) = 0 \tag{4}$$

The general solution of Eq. (4) can be expressed in terms of the Bessel functions (Conway et al., 1964)

$$y(x) = \frac{1}{x} [C_1 J_2(\lambda\sqrt{x}) + C_2 Y_2(\lambda\sqrt{x}) + C_3 I_2(\lambda\sqrt{x}) + C_4 K_2(\lambda\sqrt{x})] \tag{5}$$

$$\begin{cases} [e_1 \lambda^3 J_3(\lambda\sqrt{L_2}) + J_2(\lambda\sqrt{L_2})]C_1 + [e_1 \lambda^3 Y_3(\lambda\sqrt{L_2}) + Y_2(\lambda\sqrt{L_2})]C_2 + [e_1 \lambda^3 I_3(\lambda\sqrt{L_2}) + I_2(\lambda\sqrt{L_2})]C_3 - [e_1 \lambda^3 K_3(\lambda\sqrt{L_2}) - K_2(\lambda\sqrt{L_2})]C_4 = 0 \\ [e_2 \lambda J_4(\lambda\sqrt{L_2}) + J_3(\lambda\sqrt{L_2})]C_1 + [e_2 \lambda Y_4(\lambda\sqrt{L_2}) + Y_3(\lambda\sqrt{L_2})]C_2 + [e_2 \lambda I_4(\lambda\sqrt{L_2}) - I_3(\lambda\sqrt{L_2})]C_3 + [e_2 K_4 \lambda(\lambda\sqrt{L_2}) + K_3(\lambda\sqrt{L_2})]C_4 = 0 \\ [e_3 \lambda^3 J_3(\lambda\sqrt{L_1}) + J_2(\lambda\sqrt{L_1})]C_1 + [e_3 \lambda^3 Y_3(\lambda\sqrt{L_1}) + Y_2(\lambda\sqrt{L_1})]C_2 + [e_3 \lambda^3 I_3(\lambda\sqrt{L_1}) + I_2(\lambda\sqrt{L_1})]C_3 - [e_3 \lambda^3 K_3(\lambda\sqrt{L_1}) - K_2(\lambda\sqrt{L_1})]C_4 = 0 \\ [e_4 \lambda J_4(\lambda\sqrt{L_1}) + J_3(\lambda\sqrt{L_1})]C_1 + [e_4 \lambda Y_4(\lambda\sqrt{L_1}) + Y_3(\lambda\sqrt{L_1})]C_2 + [e_4 \lambda I_4(\lambda\sqrt{L_1}) - I_3(\lambda\sqrt{L_1})]C_3 + [e_4 K_4 \lambda(\lambda\sqrt{L_1}) + K_3(\lambda\sqrt{L_1})]C_4 = 0 \end{cases} \tag{10}$$

where  $C_1, C_2, C_3$  and  $C_4$  are constant coefficients.  $J_2$  and  $Y_2$  are the Bessel functions of the first and second kind, respectively, of order 2.  $I_2$  and  $K_2$  are the modified Bessel functions of the first and second kind, respectively, of order 2. The numerical values of the Bessel functions can be obtained easily from the mathematical software such as Matlab. Parameter  $\lambda$  in Eq. (5) is defined as

$$\lambda^4 = \frac{64\rho L_1^2 \omega^2}{Er_b^2} \tag{6}$$

$$\begin{vmatrix} e_1 \lambda^3 J_3(\lambda\sqrt{L_2}) + J_2(\lambda\sqrt{L_2}) & e_1 \lambda^3 Y_3(\lambda\sqrt{L_2}) + Y_2(\lambda\sqrt{L_2}) & e_1 \lambda^3 I_3(\lambda\sqrt{L_2}) + I_2(\lambda\sqrt{L_2}) & -[e_1 \lambda^3 K_3(\lambda\sqrt{L_2}) - K_2(\lambda\sqrt{L_2})] \\ e_2 \lambda J_4(\lambda\sqrt{L_2}) + J_3(\lambda\sqrt{L_2}) & e_2 \lambda Y_4(\lambda\sqrt{L_2}) + Y_3(\lambda\sqrt{L_2}) & e_2 \lambda I_4(\lambda\sqrt{L_2}) - I_3(\lambda\sqrt{L_2}) & e_2 K_4 \lambda(\lambda\sqrt{L_2}) + K_3(\lambda\sqrt{L_2}) \\ e_3 \lambda^3 J_3(\lambda\sqrt{L_1}) + J_2(\lambda\sqrt{L_1}) & e_3 \lambda^3 Y_3(\lambda\sqrt{L_1}) + Y_2(\lambda\sqrt{L_1}) & e_3 \lambda^3 I_3(\lambda\sqrt{L_1}) + I_2(\lambda\sqrt{L_1}) & -[e_3 \lambda^3 K_3(\lambda\sqrt{L_1}) - K_2(\lambda\sqrt{L_1})] \\ e_4 \lambda J_4(\lambda\sqrt{L_1}) + J_3(\lambda\sqrt{L_1}) & e_4 \lambda Y_4(\lambda\sqrt{L_1}) + Y_3(\lambda\sqrt{L_1}) & e_4 \lambda I_4(\lambda\sqrt{L_1}) - I_3(\lambda\sqrt{L_1}) & e_4 K_4 \lambda(\lambda\sqrt{L_1}) + K_3(\lambda\sqrt{L_1}) \end{vmatrix} = 0 \tag{12}$$

Under the assumption of small deformation and small rotation (since such fine movements appear to be more than adequate for the rat to be able to discriminate fine detail such as texture (Carvell and Simons, 1990)), the slope  $\theta(x)$  of the transverse displacement curve, bending moment  $M(x)$  and shear force  $S(x)$  at any location can be derived as

$$\begin{cases} \theta(x) = \frac{dy}{dx} = -\frac{\lambda}{2x^{3/2}} [C_1 J_3(\lambda\sqrt{x}) + C_2 Y_3(\lambda\sqrt{x}) - C_3 I_3(\lambda\sqrt{x}) + C_4 K_3(\lambda\sqrt{x})] \\ M(x) = EI \frac{d^2 y}{dx^2} = \frac{\pi r_b^4 \lambda^2 x^2 E}{16 I_1^4} [C_1 J_4(\lambda\sqrt{x}) + C_2 Y_4(\lambda\sqrt{x}) + C_3 I_4(\lambda\sqrt{x}) + C_4 K_4(\lambda\sqrt{x})] \\ S(x) = \frac{d}{dx} \left( EI \frac{d^2 y}{dx^2} \right) = \frac{\pi r_b^4 \lambda^3 x^{3/2} E}{32 I_1^4} [C_1 J_3(\lambda\sqrt{x}) + C_2 Y_3(\lambda\sqrt{x}) + C_3 I_3(\lambda\sqrt{x}) - C_4 K_3(\lambda\sqrt{x})] \end{cases} \tag{7}$$

This study focuses on solution of the natural vibration frequency. The procedure is to apply boundary conditions to determine  $\lambda$  and then the natural frequency  $f$  can be obtained from

Eqs. (3) and (6). The solutions of the natural frequency for a range of boundary conditions are discussed in Section 3.

### 3. Natural frequency $f$

#### 3.1. Frequency equation

The spring constraints illustrated in Fig. 1(c) can be described as follows:

At the tip,  $x = L_2$  and

$$S = -k_t y(x) \text{ and } M = T_t \theta \tag{8}$$

At the base,  $x = L_1$  and

$$S = -k_b y(x) \text{ and } M = T_b \theta \tag{9}$$

Applying boundary conditions (8) and (9) to Eqs. (5) and (7) results in a set of simultaneous equations with respect to  $C_1, C_2, C_3$  and  $C_4$

where

$$\varepsilon_1 = \frac{\pi r_b^4 L_2^{5/2} E}{32 k_t L_1^4}, \quad \varepsilon_2 = \frac{\pi r_b^4 L_2^{7/2} E}{8 T_t L_1^4}, \quad \varepsilon_3 = \frac{\pi r_b^4 E}{32 k_b L_1^{3/2}}, \quad \varepsilon_4 = \frac{\pi r_b^4 E}{8 T_b L_1^{1/2}} \tag{11}$$

According to mathematics, to have non-zero solutions for  $C_1, C_2, C_3$  and  $C_4$ , the determinant consisted of the coefficients of Eq. (10) must be zero, i.e.,

For a given problem,  $\lambda$  can be numerically obtained from Eq. (12). Then, by applying Eqs. (3) and (6), the natural frequency  $f$  can be determined. Therefore, Eq. (12) is also called the frequency equation.

#### 3.2. Dimensional analysis for natural frequency $f$

Before discussing the solution of the frequency equation (Eq. (12)), dimensional analysis was carried out to understand the functional relationship between the natural frequency  $f$  and other parameters. The natural frequency  $f$  depends on the elastic modulus  $E$  and the density  $\rho$  of the rat whisker material, the geometrical parameters  $r_b, r_t$  and  $L$  as well as the translational spring stiffness  $k_t, k_b$  and the rotational spring stiffness  $T_t, T_b$  at the

boundaries, i.e.,

$$f = f(r_t, r_b, L, E, \rho, k_t, k_b, T_t, T_b) \tag{13}$$

According to the Buckingham  $\Pi$  theorem for dimensional analysis (Buckingham, 1914), the number of parameters can be reduced based on the number of fundamental dimensions presented in the physical problem by using dimensionless parameters. For this purpose,  $L, E$  and  $\rho$  are chosen as the primary quantities that express all the fundamental dimensions of the physical problem ( $m, N, s$ ). The natural frequency  $f$  can be expressed by the dimensionless function  $\Pi_f$  as

$$f = \frac{1}{L} \sqrt{\frac{E}{\rho}} \Pi_f \left( \frac{r_t}{L}, \frac{r_b}{L}, \frac{k_t}{EL}, \frac{k_b}{EL}, \frac{T_t}{EL^3}, \frac{T_b}{EL^3} \right) \tag{14}$$

Eq. (14) shows that the natural frequency  $f$  of the rat whisker is always inversely proportional to the square root of the density of the whisker material because the dimensionless function  $\Pi_f$  is independent of the density. This conclusion from the simple dimensional analysis can be applied to any boundary condition and this is confirmed by the considerations of all the special cases in following subsections.

### 3.3. General formula and numerical solutions of $f$ for classical boundary conditions

As noted above, Eq. (12) is the frequency equation for the generic boundary conditions with elastic support at the ends. The classical boundary constraint conditions, such as free, simply supported (pinned), sliding and fixed constraints, can be treated as special cases. In terms of the application to rat whiskers, in an experiment either the tip or the base can be rigidly clamped (i.e., fixed), meaning that both the translational and the rotational springs have an infinite stiffness. In the situation of the rat whisker moving freely in air, the tip should be treated as a free end in the beam model, which means that the springs connected to the tip have a zero stiffness value. Before dealing with the problem with the generic boundary conditions, the solutions of the natural frequency for these classical boundary conditions are discussed.

In the case of free tip and fixed base (shortened as free–fixed) boundary conditions,  $k_t = T_t = 0$  and  $k_b = T_b = \infty$ , the frequency equation can be generated from Eq. (12) as

$$\begin{vmatrix} J_3(\lambda\sqrt{L_2}) & Y_3(\lambda\sqrt{L_2}) & I_3(\lambda\sqrt{L_2}) & -K_3(\lambda\sqrt{L_2}) \\ J_4(\lambda\sqrt{L_2}) & Y_4(\lambda\sqrt{L_2}) & I_4(\lambda\sqrt{L_2}) & K_4(\lambda\sqrt{L_2}) \\ J_2(\lambda\sqrt{L_1}) & Y_2(\lambda\sqrt{L_1}) & I_2(\lambda\sqrt{L_1}) & K_2(\lambda\sqrt{L_1}) \\ J_3(\lambda\sqrt{L_1}) & Y_3(\lambda\sqrt{L_1}) & -I_3(\lambda\sqrt{L_1}) & K_3(\lambda\sqrt{L_1}) \end{vmatrix} = 0 \tag{15}$$

It can be seen that Eq. (15) is independent of material properties. Therefore, the unknown variable  $\lambda$ , i.e., the root of Eq. (15), is independent of  $E$  or  $\rho$  and furthermore,  $\lambda$  only depends on the other two parameters  $L_2$  and  $L_1$  in Eq. (15), i.e.,

$$\lambda = \lambda(L_2, L_1) \tag{16}$$

According to Eq. (6),  $\lambda$  has the dimension of (length)<sup>-0.5</sup>. Following the Buckingham  $\Pi$  theorem in dimensional analysis, we have

$$\lambda\sqrt{L_1} = \Pi_\lambda \left( \frac{L_2}{L_1} \right) \tag{17}$$

Eq. (17) indicates that  $\lambda\sqrt{L_1}$ , therefore,  $\lambda^2 L_1$  only depends on  $L_2/L_1$ , i.e.,  $r_t/r_b$  (as  $r_t/r_b = L_2/L_1$ , see Fig. 1(b)). According to Eqs. (3), (6) and (17), the natural frequency can be expressed as

$$f = \alpha \frac{r_b}{L^2} \sqrt{\frac{E}{\rho}} \tag{18}$$

where  $\alpha = (\lambda^2 L_1 / 16\pi)(1 - (r_t/r_b))^2$  only depends on  $r_t/r_b$ . Note that  $L$

in Eq. (18) is the length of the truncated cone. The functional relationship between  $\alpha$  and  $r_t/r_b$  can be obtained numerically through finding the non-zero roots for  $\lambda$  from Eq. (15). For a given ratio  $r_t/r_b$ , the first non-zero root  $\lambda_1$  of Eq. (15) leads to the first non-zero value  $\alpha_1$ , which gives the first natural frequency  $f_1$  of the truncated cone under the free–fixed (for free tip and fixed base) boundary conditions. The second non-zero root  $\lambda_2$  corresponds to the second non-zero value  $\alpha_2$  and the second natural frequency  $f_2$ , etc. The numerical results of the first three natural frequency coefficients  $\alpha_1, \alpha_2$  and  $\alpha_3$  are shown in Fig. 2(a)–(c) where it can be seen that for a cylindrical beam ( $r_t/r_b = 1$ ),  $\alpha_1 = 0.2798$  and for a fully conical beam ( $r_t/r_b = 0$ ),  $\alpha_1 = 0.6938$ . These values are consistent with literature (see, Conway et al. 1964; Georgian, 1965; Weaver et al. 1990).

Similarly, it can be derived that Eq. (18) applies to all the classical free, pinned, fixed or sliding constraints at the ends of a truncated conical beam (note that a sliding constraint corresponds to a translational spring with zero stiffness and a rotational spring with infinite stiffness). It can also be concluded from similar dimensional analysis that the parameter  $\alpha$  only depends on  $r_t/r_b$  in all the classical cases. It is worth noting that a formula similar to Eq. (18) for some combinations of the classical boundary conditions can be found in the literature, (e.g., Conway et al. 1964; Georgian, 1965; Sanger, 1967; Weaver et al. 1990). To the best of our knowledge, no proof of Eq. (18) has been provided previously. The dependencies of  $\alpha_1, \alpha_2$  and  $\alpha_3$  on  $r_t/r_b$  are numerically obtained and illustrated in Fig. 2(a), (b) and (c), respectively, for the 16 combinations of the classical boundary conditions for the whisker tip and for the whisker base. These curves can be fitted very well by different polynomial functions, which are listed in Tables 1–3. The results presented in Fig. 2 and Tables 1–3 provide a useful database for determining the first three natural frequencies of a truncated conical beam under the combinations of the classical boundary conditions.

## 4. Natural frequency of rat whiskers

Eq. (14) shows that the natural (resonance) frequency depends on the boundary conditions. In *ex vivo* experiments on whiskers, the boundary conditions can be generally described by one of the combinations of the classical boundary conditions and Fig. 2 or Tables 1–3 can then be directly applied to find the first three natural frequencies. However, in a living rat, a rat whisker is embedded at its base in a follicle–sinus complex. Instead of considering a fixed base, the constraints from the follicle on the base should be better simulated as elastic in both rotational and transverse directions (Hartmann et al., 2003). Furthermore, a rat could actively control the follicle–sinus complex to adjust the constraints on the whisker base thereby altering the natural frequencies. Here we carry out a theoretical study to investigate the influence of the base constraints on the natural frequencies of a rat whisker. The constraints at the base are simulated by the rotational and the translational springs, as illustrated in Fig. 1. The results should assist the understanding on how the natural frequencies can be adjusted through changing the stiffness values at the base.

With regard to the constraints on the whisker tip, two situations are considered. The first situation is that the rat whisker is freely whisking in air, corresponding to a free tip condition. The second situation is that the rat whisker tip is touching and sticking on an object, which is simulated as a pinned tip with  $k_t = \infty$ . Referring to Eq. (14), the natural frequency of a rat whisker depends not only on the end constraints but also on the geometry and the material properties. The geometry of rat whiskers varies from whisker to whisker even in the same rat. The material properties, including the elastic modulus, may vary within each whisker, as well as between whiskers, as found by Quist et al. (2011). A prototypical rat whisker

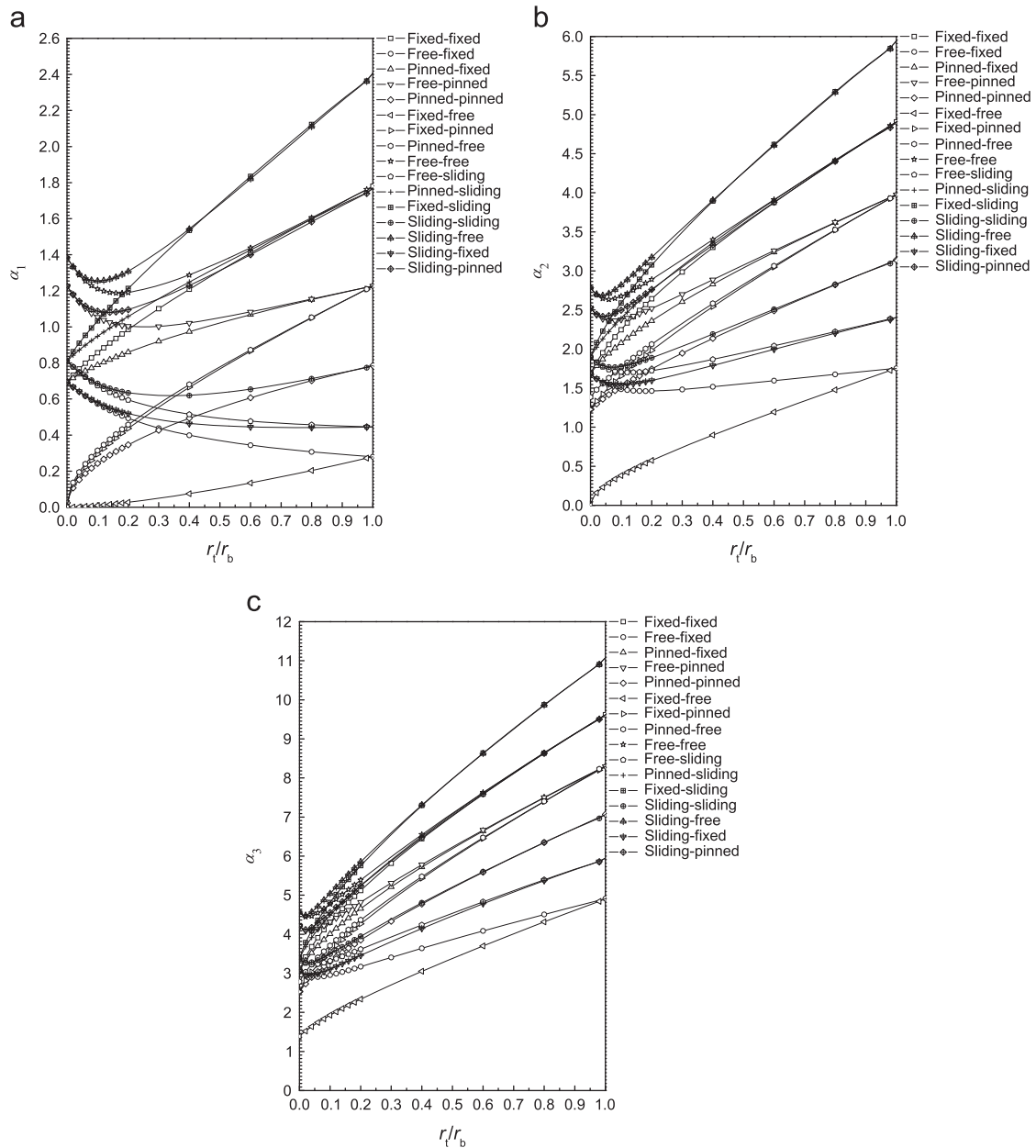


**Fig. 2.** The natural frequency coefficient  $\alpha$  as a function of the radius ratio  $r_t/r_b$  of a truncated conical beam. Each curve is for a different pair of boundary conditions denoting the condition for the tip (before the hyphen symbol) and for the base of the whisker (after the hyphen symbol), e.g., free–fixed=free tip and fixed base: (a) the first natural frequency coefficient  $\alpha_1$ ; (b) the second natural frequency coefficient  $\alpha_2$ ; and (c) the third natural frequency coefficient  $\alpha_3$ .

was generated by taking the mean values of the 18 macrovibrissae of a Sprague Dawley rat measured by Neimark et al. (2003). These values are:  $L=34.1$  mm,  $r_b=0.062$  mm,  $r_t=0.007$  mm and  $\rho=1.4$  mg/mm<sup>3</sup>. The elastic modulus of the rat whisker material was taken as 3 GPa, which is within the range of reported data from 1.4 GPa to 7.8 GPa (Neimark et al., 2003; Hartmann et al., 2003; Herzog et al., 2005; Birdwell et al., 2007; Quist et al. 2011; Carl et al., 2012).

Fig. 3(a), (b) and (c) shows numerical results for the first, second and third natural frequencies, respectively, of the prototypical rat whisker when freely whisking in air. As indicated by the labels in the figures, when both of the stiffness  $k_b$  and  $T_b$  approach either extremely large or extremely small values, the elastic constraints at the base approach the classic boundary conditions such as free, pinned, sliding or fixed boundaries. All the frequencies in the extreme conditions reported in Fig. 3 agree with those shown in Fig. 2. For example, when  $k_b$  reduces from  $10^{-3}$  to  $10^{-9}$

N/m and  $T_b$  increases from  $10^{-4}$  to  $10^{-3}$  Nm, Fig. 3 shows that the first three natural frequencies reach respectively to their lower bounds of 44, 116 and 234 Hz. These are the exact same values as can be calculated from Fig. 2 and Eq. (18) under free–fixed conditions.

Fig. 3(a) shows the first natural frequency of the prototypical rat whisker ranges from 44 to 94 Hz, which is in line with experimental data in literature. For instance, Hartmann et al. (2003) reported the first natural frequencies of the D row rat whiskers as being between 50 and 128 Hz based on experimental tests conducted with whiskers kept in the free–fixed boundary conditions. The measured first natural frequencies by Neimark et al. (2003) for the  $\beta$ ,  $C_1$ , and  $C_2$  whiskers under either *in vivo* or *ex vivo* condition, with whiskers in the free–fixed boundary condition, also agree with the results in Fig. 3 (see Table 1 of Neimark et al., 2003). The predicted second natural frequencies of

**Table 1**  
Fitted functions for the first natural frequency coefficient  $\alpha_1$  with different boundary conditions.

Boundary conditions	Fitted function	$R^2$
Fixed–fixed	$-0.7909\left(\frac{L}{r_b}\right)^4 + 1.9194\left(\frac{L}{r_b}\right)^3 - 1.8246\left(\frac{L}{r_b}\right)^2 + 1.7478\left(\frac{L}{r_b}\right) + 0.6938$	0.9999
Free–fixed	$-0.885\left(\frac{L}{r_b}\right)^4 - 2.4022\left(\frac{L}{r_b}\right)^3 + 2.5267\left(\frac{L}{r_b}\right)^2 - 1.4218\left(\frac{L}{r_b}\right) + 0.6938$	0.9999
Pinned–fixed	$-0.5251\left(\frac{L}{r_b}\right)^4 + 1.3207\left(\frac{L}{r_b}\right)^3 - 1.3035\left(\frac{L}{r_b}\right)^2 + 1.038\left(\frac{L}{r_b}\right) + 0.6938$	0.9999
Free–pinned	$-5.0358\left(\frac{L}{r_b}\right)^5 + 15.209\left(\frac{L}{r_b}\right)^4 - 17.696\left(\frac{L}{r_b}\right)^3 + 10.061\left(\frac{L}{r_b}\right)^2 - 2.5378\left(\frac{L}{r_b}\right) + 1.226$	0.9994
Pinned–pinned	$-28.289\left(\frac{L}{r_b}\right)^6 + 90.154\left(\frac{L}{r_b}\right)^5 - 110.67\left(\frac{L}{r_b}\right)^4 + 66.013\left(\frac{L}{r_b}\right)^3 - 20.236\left(\frac{L}{r_b}\right)^2 + 3.7917\left(\frac{L}{r_b}\right) + 0.0167$	0.998
Fixed–free	$0.1026\left(\frac{L}{r_b}\right)^4 - 0.2916\left(\frac{L}{r_b}\right)^3 + 0.4025\left(\frac{L}{r_b}\right)^2 + 0.0671\left(\frac{L}{r_b}\right) + 0.0007$	1
Fixed–pinned	$-24.204\left(\frac{L}{r_b}\right)^6 + 78.209\left(\frac{L}{r_b}\right)^5 - 97.64\left(\frac{L}{r_b}\right)^4 + 59.413\left(\frac{L}{r_b}\right)^3 - 18.577\left(\frac{L}{r_b}\right)^2 + 3.9849\left(\frac{L}{r_b}\right) + 0.0365$	0.9993
Pinned–free	$15.839\left(\frac{L}{r_b}\right)^5 - 42.777\left(\frac{L}{r_b}\right)^4 + 42.161\left(\frac{L}{r_b}\right)^3 - 18.669\left(\frac{L}{r_b}\right)^2 + 4.6861\left(\frac{L}{r_b}\right)$	0.9961
Free–free	$3.6376\left(\frac{L}{r_b}\right)^4 - 9.0666\left(\frac{L}{r_b}\right)^3 + 8.0687\left(\frac{L}{r_b}\right)^2 - 2.2267\left(\frac{L}{r_b}\right) + 1.3689$	0.9975
Free–sliding	$1.2481\left(\frac{L}{r_b}\right)^4 - 3.3228\left(\frac{L}{r_b}\right)^3 + 3.3363\left(\frac{L}{r_b}\right)^2 - 1.6221\left(\frac{L}{r_b}\right) + 0.808$	0.9998
Pinned–sliding	$-0.568\left(\frac{L}{r_b}\right)^4 + 1.4681\left(\frac{L}{r_b}\right)^3 - 1.3977\left(\frac{L}{r_b}\right)^2 + 1.4499\left(\frac{L}{r_b}\right) + 0.8145$	1
Sliding–sliding	$-2.2377\left(\frac{L}{r_b}\right)^5 + 7.0068\left(\frac{L}{r_b}\right)^4 - 8.6381\left(\frac{L}{r_b}\right)^3 + 5.5427\left(\frac{L}{r_b}\right)^2 - 1.6988\left(\frac{L}{r_b}\right) + 0.8094$	0.9998
Fixed–sliding	$-0.8416\left(\frac{L}{r_b}\right)^4 + 2.1421\left(\frac{L}{r_b}\right)^3 - 2.0341\left(\frac{L}{r_b}\right)^2 + 2.3207\left(\frac{L}{r_b}\right) + 0.8175$	1
Sliding–free	$-8.7042\left(\frac{L}{r_b}\right)^5 + 25.506\left(\frac{L}{r_b}\right)^4 - 28.27\left(\frac{L}{r_b}\right)^3 + 14.902\left(\frac{L}{r_b}\right)^2 - 2.4076\left(\frac{L}{r_b}\right) + 1.3752$	0.9998
Sliding–fixed	$1.1565\left(\frac{L}{r_b}\right)^4 - 3.0382\left(\frac{L}{r_b}\right)^3 + 3.0001\left(\frac{L}{r_b}\right)^2 - 1.3623\left(\frac{L}{r_b}\right) + 0.6915$	0.9996
Sliding–pinned	$-6.5804\left(\frac{L}{r_b}\right)^5 + 19.511\left(\frac{L}{r_b}\right)^4 - 22.021\left(\frac{L}{r_b}\right)^3 + 11.926\left(\frac{L}{r_b}\right)^2 - 2.2907\left(\frac{L}{r_b}\right) + 1.2194$	0.9997

**Table 2**  
Fitted functions for the second natural frequency coefficient  $\alpha_2$  with different boundary conditions.

Boundary conditions	Fitted function	$R^2$
Fixed–fixed	$-4.0943\left(\frac{L}{r_b}\right)^4 + 9.8166\left(\frac{L}{r_b}\right)^3 - 8.6832\left(\frac{L}{r_b}\right)^2 + 6.1564\left(\frac{L}{r_b}\right) + 1.6827$	0.9998
Free–fixed	$4.8948\left(\frac{L}{r_b}\right)^4 - 11.4\left(\frac{L}{r_b}\right)^3 + 9.111\left(\frac{L}{r_b}\right)^2 - 2.5069\left(\frac{L}{r_b}\right) + 1.6827$	0.9795
Pinned–fixed	$-2.7158\left(\frac{L}{r_b}\right)^4 + 6.5573\left(\frac{L}{r_b}\right)^3 - 5.8771\left(\frac{L}{r_b}\right)^2 + 4.3104\left(\frac{L}{r_b}\right) + 1.6827$	0.9998
Free–pinned	$-19.98\left(\frac{L}{r_b}\right)^5 + 55.513\left(\frac{L}{r_b}\right)^4 - 56.779\left(\frac{L}{r_b}\right)^3 + 26.086\left(\frac{L}{r_b}\right)^2 - 3.3838\left(\frac{L}{r_b}\right) + 2.5099$	0.9985
Pinned–pinned	$0.9344\left(\frac{L}{r_b}\right)^3 - 1.9143\left(\frac{L}{r_b}\right)^2 + 2.8959\left(\frac{L}{r_b}\right) + 1.2387$	0.9977
Fixed–free	$17.838\left(\frac{L}{r_b}\right)^5 - 48.08\left(\frac{L}{r_b}\right)^4 + 47.189\left(\frac{L}{r_b}\right)^3 - 20.699\left(\frac{L}{r_b}\right)^2 + 5.5188\left(\frac{L}{r_b}\right)$	0.9977
Fixed–pinned	$1.2222\left(\frac{L}{r_b}\right)^3 - 2.6091\left(\frac{L}{r_b}\right)^2 + 4.1123\left(\frac{L}{r_b}\right) + 1.2598$	0.9998
Pinned–free	$0.9978\left(\frac{L}{r_b}\right)^3 - 2.0579\left(\frac{L}{r_b}\right)^2 + 3.6322\left(\frac{L}{r_b}\right) + 1.413$	0.9999
Free–free	$52.733\left(\frac{L}{r_b}\right)^6 - 173.96\left(\frac{L}{r_b}\right)^5 + 223.09\left(\frac{L}{r_b}\right)^4 - 140.26\left(\frac{L}{r_b}\right)^3 + 44.769\left(\frac{L}{r_b}\right)^2 - 4.2183\left(\frac{L}{r_b}\right) + 2.7648$	0.9998
Free–sliding	$4.9776\left(\frac{L}{r_b}\right)^4 - 11.696\left(\frac{L}{r_b}\right)^3 + 9.5291\left(\frac{L}{r_b}\right)^2 - 2.2452\left(\frac{L}{r_b}\right) + 1.8584$	0.9951
Pinned–sliding	$-2.7581\left(\frac{L}{r_b}\right)^4 + 6.8143\left(\frac{L}{r_b}\right)^3 - 6.2795\left(\frac{L}{r_b}\right)^2 + 5.201\left(\frac{L}{r_b}\right) + 1.9229$	0.9999
Sliding–sliding	$-12.274\left(\frac{L}{r_b}\right)^5 + 35.224\left(\frac{L}{r_b}\right)^4 - 37.408\left(\frac{L}{r_b}\right)^3 + 18.064\left(\frac{L}{r_b}\right)^2 - 2.3273\left(\frac{L}{r_b}\right) + 1.8676$	0.9983
Fixed–sliding	$-3.9622\left(\frac{L}{r_b}\right)^4 + 9.8441\left(\frac{L}{r_b}\right)^3 - 9.098\left(\frac{L}{r_b}\right)^2 + 7.2097\left(\frac{L}{r_b}\right) + 1.94$	0.9999
Sliding–free	$-21.079\left(\frac{L}{r_b}\right)^5 + 58.106\left(\frac{L}{r_b}\right)^4 - 58.343\left(\frac{L}{r_b}\right)^3 + 25.537\left(\frac{L}{r_b}\right)^2 - 1.0132\left(\frac{L}{r_b}\right) + 2.7208$	0.9995
Sliding–fixed	$-10.901\left(\frac{L}{r_b}\right)^5 + 30.935\left(\frac{L}{r_b}\right)^4 - 32.672\left(\frac{L}{r_b}\right)^3 + 15.827\left(\frac{L}{r_b}\right)^2 - 2.4552\left(\frac{L}{r_b}\right) + 1.6636$	0.9991
Sliding–pinned	$-19.201\left(\frac{L}{r_b}\right)^5 + 52.964\left(\frac{L}{r_b}\right)^4 - 53.424\left(\frac{L}{r_b}\right)^3 + 23.682\left(\frac{L}{r_b}\right)^2 - 1.6026\left(\frac{L}{r_b}\right) + 2.4732$	0.9994

this prototypical rat whisker are in the range of 116–212 Hz (Fig. 3(b)) and predicted third natural frequencies are in the range of 234–381 Hz (Fig. 3(c)). Hartmann et al. (2003) reported that a  $C_1$  rat

whisker under free–fixed conditions has the first three natural frequencies of 40, 94 and 188 Hz. Note that the lowest values of the predicted ranges of our study correspond to free–fixed

**Table 3**  
Fitted functions for the third natural frequency coefficient  $\alpha_3$  with different boundary conditions.

Boundary conditions	Fitted functions	$R^2$
Fixed–fixed	$-10.671\left(\frac{r_b}{r_t}\right)^4 + 25.25\left(\frac{r_b}{r_t}\right)^3 - 21.744\left(\frac{r_b}{r_t}\right)^2 + 13.642\left(\frac{r_b}{r_t}\right) + 3.06$	0.9996
Free–fixed	$9.2448\left(\frac{r_b}{r_t}\right)^4 - 20.415\left(\frac{r_b}{r_t}\right)^3 + 14.704\left(\frac{r_b}{r_t}\right)^2 - 1.6035\left(\frac{r_b}{r_t}\right) + 3.06$	0.9953
Pinned–fixed	$-7.409\left(\frac{r_b}{r_t}\right)^4 + 17.66\left(\frac{r_b}{r_t}\right)^3 - 15.45\left(\frac{r_b}{r_t}\right)^2 + 10.379\left(\frac{r_b}{r_t}\right) + 3.06$	0.9997
Free–pinned	$-35.602\left(\frac{r_b}{r_t}\right)^5 + 95.404\left(\frac{r_b}{r_t}\right)^4 - 92.148\left(\frac{r_b}{r_t}\right)^3 + 37.887\left(\frac{r_b}{r_t}\right)^2 - 1.4249\left(\frac{r_b}{r_t}\right) + 4.1602$	0.9997
Pinned–pinned	$-5.5313\left(\frac{r_b}{r_t}\right)^4 + 13.221\left(\frac{r_b}{r_t}\right)^3 - 11.62\left(\frac{r_b}{r_t}\right)^2 + 8.4313\left(\frac{r_b}{r_t}\right) + 2.551$	0.9989
Fixed–free	$1.5046\left(\frac{r_b}{r_t}\right)^3 - 3.1567\left(\frac{r_b}{r_t}\right)^2 + 5.142\left(\frac{r_b}{r_t}\right)^1 + 1.4295$	0.9998
Fixed–pinned	$-6.5005\left(\frac{r_b}{r_t}\right)^4 + 15.925\left(\frac{r_b}{r_t}\right)^3 - 14.493\left(\frac{r_b}{r_t}\right)^2 + 10.746\left(\frac{r_b}{r_t}\right) + 2.6023$	0.9998
Pinned–free	$2.9976\left(\frac{r_b}{r_t}\right)^3 - 6.1498\left(\frac{r_b}{r_t}\right)^2 + 8.6021\left(\frac{r_b}{r_t}\right)^1 + 2.8814$	0.9996
Free–free	$87.144\left(\frac{r_b}{r_t}\right)^6 - 285.02\left(\frac{r_b}{r_t}\right)^5 + 358.83\left(\frac{r_b}{r_t}\right)^4 - 216.76\left(\frac{r_b}{r_t}\right)^3 + 62.73\left(\frac{r_b}{r_t}\right)^2 - 1.7622\left(\frac{r_b}{r_t}\right) + 4.4885$	0.9998
Free–sliding	$7.7409\left(\frac{r_b}{r_t}\right)^4 - 17.158\left(\frac{r_b}{r_t}\right)^3 + 12.372\left(\frac{r_b}{r_t}\right)^2 - 0.2395\left(\frac{r_b}{r_t}\right) + 3.2576$	0.9983
Pinned–sliding	$-6.86\left(\frac{r_b}{r_t}\right)^4 + 16.905\left(\frac{r_b}{r_t}\right)^3 - 15.467\left(\frac{r_b}{r_t}\right)^2 + 11.583\left(\frac{r_b}{r_t}\right) + 3.4501$	0.9998
Sliding–sliding	$-23.329\left(\frac{r_b}{r_t}\right)^5 + 63.125\left(\frac{r_b}{r_t}\right)^4 - 61.563\left(\frac{r_b}{r_t}\right)^3 + 25.352\left(\frac{r_b}{r_t}\right)^2 + 0.1819\left(\frac{r_b}{r_t}\right) + 3.281$	0.9995
Fixed–sliding	$-9.2506\left(\frac{r_b}{r_t}\right)^4 + 22.981\left(\frac{r_b}{r_t}\right)^3 - 21.018\left(\frac{r_b}{r_t}\right)^2 + 14.845\left(\frac{r_b}{r_t}\right) + 3.4937$	0.9997
Sliding–free	$94.108\left(\frac{r_b}{r_t}\right)^6 - 300.41\left(\frac{r_b}{r_t}\right)^5 + 367.3\left(\frac{r_b}{r_t}\right)^4 - 213.16\left(\frac{r_b}{r_t}\right)^3 + 57.209\left(\frac{r_b}{r_t}\right)^2 + 1.5766\left(\frac{r_b}{r_t}\right) + 4.4713$	0.9998
Sliding–fixed	$-20.936\left(\frac{r_b}{r_t}\right)^5 + 57.276\left(\frac{r_b}{r_t}\right)^4 - 56.696\left(\frac{r_b}{r_t}\right)^3 + 23.937\left(\frac{r_b}{r_t}\right)^2 - 0.6378\left(\frac{r_b}{r_t}\right) + 2.9852$	0.9993
Sliding–pinned	$85.748\left(\frac{r_b}{r_t}\right)^6 - 276.39\left(\frac{r_b}{r_t}\right)^5 + 341.41\left(\frac{r_b}{r_t}\right)^4 - 200.71\left(\frac{r_b}{r_t}\right)^3 + 55.115\left(\frac{r_b}{r_t}\right)^2 + 0.3315\left(\frac{r_b}{r_t}\right) + 4.1246$	0.9996

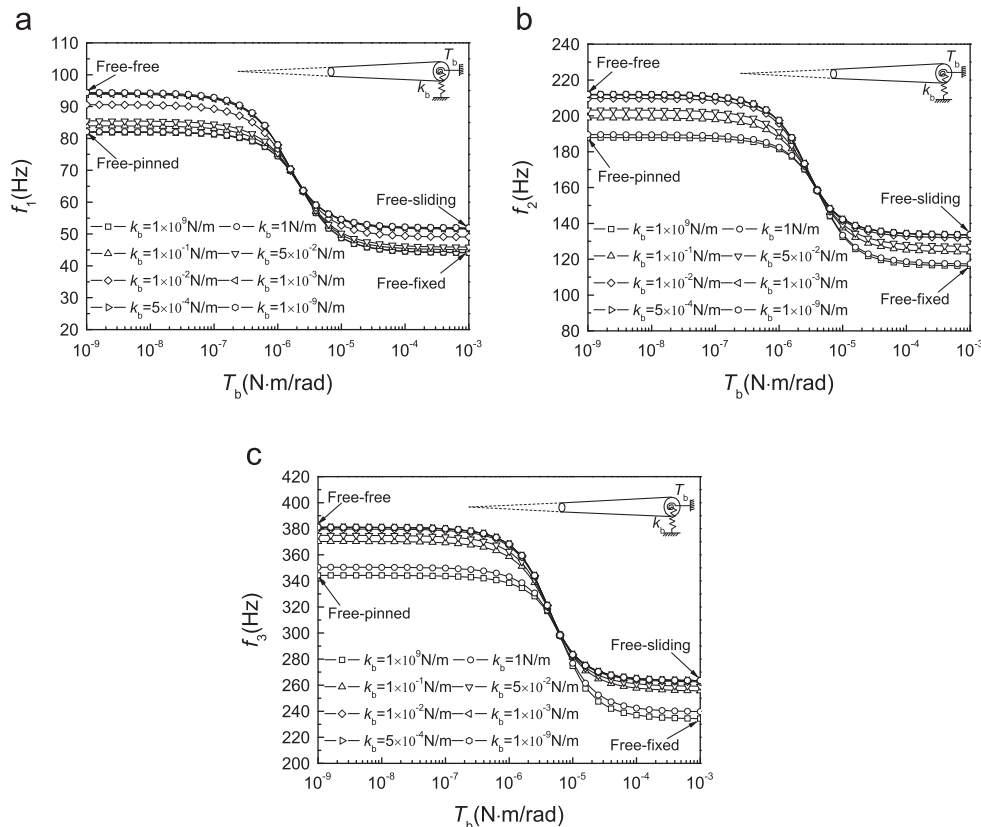


**Fig. 3.** The natural frequencies of a representative rat whisker freely whisking in air under different elastic constraining stiffnesses  $k_b$  and  $T_b$  at the base: (a) the first natural frequency; (b) the second natural frequency; and (c) the third natural frequency.

conditions, as shown in Fig. 3. Given that the input data from the prototypical whisker used for the prediction are not identical to those for the experimental whiskers, we believe that the difference

between theoretical prediction and experimental data is understandable and acceptable. This comparison with experimental data provides us the confidence that the established truncated conical

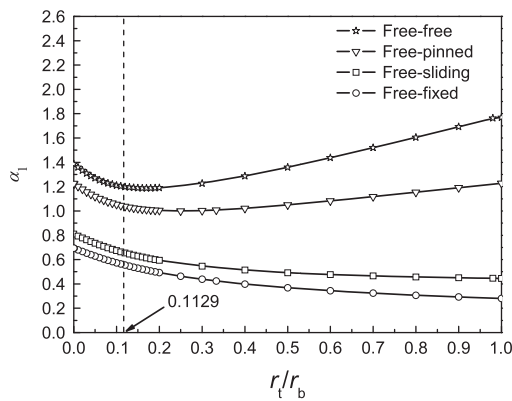


Fig. 4. The natural frequency coefficient  $\alpha_1$  for four special boundary conditions.

model has the capacity to model and analyse the natural frequencies of rat whiskers.

Fig. 3 shows that all three natural frequencies decrease with an increase in either transverse stiffness  $k_b$  or rotational stiffness  $T_b$ . This finding is also consistent with the results from Fig. 2. To clearly illustrate this agreement, Fig. 4 is extracted directly from Fig. 2(a) for the first natural frequency coefficient  $\alpha_1$ . For a given radius ratio  $r_t/r_b$  (here it is about 0.1129), Fig. 4 shows that  $\alpha_1$ , i.e., the first natural frequency for a given whisker, decreases in the order from free-free, to free-pinned, free-sliding and free-fixed boundary conditions, in correspondence to the jumping increase of  $k_b$  and/or  $T_b$  from zero to infinite.

The most interesting finding from Fig. 3 is that all the three natural frequencies are very sensitive to the rotational stiffness  $T_b$  within a certain range. For the first natural frequency, the sensitive range of  $T_b$  is  $3 \times 10^{-7}$ – $10^{-5}$  Nm. It is  $7 \times 10^{-7}$ – $10^{-5}$  Nm for the second natural frequency and  $10^{-6}$ – $2 \times 10^{-5}$  Nm for the third natural frequency. Within these ranges, the corresponding natural frequency decreases quickly with the increase in  $T_b$  and the frequency is generally insensitive to the change of  $k_b$ . For example, the first natural frequency  $f_1$  can change from about 88 to 48 Hz if  $T_b$  increases from  $3 \times 10^{-7}$  to  $10^{-5}$  Nm. This means that the rat could easily adjust the natural frequencies of individual whiskers by increasing or decreasing the rotational constraint at the whisker base. According to the physiology, the whiskers are supported by the follicle–sinus complexes which act as controllable bearing through control by surrounding intrinsic muscles (Szwed and Bagdasarian, 2003). Therefore, it is practically feasible for the rat to control the natural frequency of individual whiskers over a wide range by adjusting the rotational constraint at the base. This finding provides support for the theory that whisker resonance could be used to discriminate textures (Neimark et al., 2003; Hartmann et al., 2003; Moore, 2004; Moore and Andermann, 2005).

The numerical results of Fig. 3 are obtained from a single prototypical rat whisker. To confirm that a controllable zone for the natural frequency exists through adjustment of the rotational constraint at the base, the first natural frequencies of all 18 whiskers in Table 2 of Neimark et al. (2003) were calculated by using the measured data of  $L$ ,  $r_t/r_b$  and  $\rho$  presented in that table and assuming  $E=3$  GPa for all the whiskers. The predicted results, in Fig. 5, clearly show that the first natural frequency of all 18 whiskers is sensitive to the rotational stiffness within a certain range although the range can be different for different whiskers. Fig. 5 also indicates that the first natural frequency of all 18 whiskers under free–fixed conditions used in that study is within the range of 31–54 Hz.

Considering the second situation of the rat whisker tip touching and sticking to an object (the so-called “stick-slip” behaviour), the boundary condition at the tip is simulated as pinned and the base in the follicle–sinus complex is constrained by both the transverse

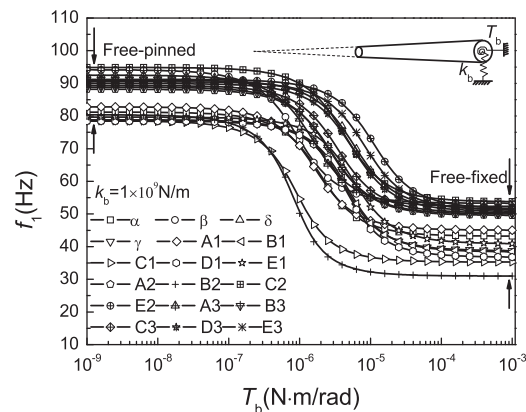


Fig. 5. The natural frequency  $f_1$  for 18 whiskers with  $k_b = 1 \times 10^9$  N/m.

spring  $k_b$  and the rotational spring  $T_b$ . Fig. 6(a), (b) and (c) shows the numerical results of the first, second and third natural frequencies of the representative rat whisker, respectively. As the tip is now pinned, comparing to Fig. 3, the values of the natural frequencies are higher. Other than that, all the findings from Fig. 3 can also be observed from Fig. 6. In this situation, there also exists a window in which the natural frequencies of the rat whiskers can be easily changed by adjustment of the rotational spring stiffness  $T_b$  alone.

## 5. Conclusions

A truncated conical beam model with generic elastic constraints in both transverse and rotational directions at the ends was developed to study the vibration of rat whiskers with emphasis on predicting the natural resonant frequency. Applying an established theoretical model to the whiskers, the natural frequencies of the whiskers were predicted for two typical situations: freely whisking in air and with the tip contacting and sticking to an object. Our major findings are summarised below:

- Dimensional analysis proves that the natural frequency of a truncated conical beam with generic spring constraints is inversely proportional to the square root of the mass density,  $f \propto \sqrt{1/\rho}$ .
- Under all combinations of the classical four boundary conditions for the ends of a truncated conical beam, namely free, pinned, fixed or sliding boundary conditions, it was proven that the natural frequency can be expressed as  $f = \alpha(r_b/L^2)\sqrt{E/\rho}$  and the coefficient  $\alpha$  only depends on the ratio of the radii at the tip and at the base of the beam, i.e.,  $\alpha = \alpha(r_t/r_b)$ .
- Our numerical results show that there exists a window where the natural frequency of a rat whisker is sensitive to the change of the rotational constraint at the base. This indicates that the natural frequency of a rat whisker can be adjusted within a wide range in a behaving animal, by manipulating the constraints of the follicle into which the whisker is inserted at its base. This has implications for the concept of texture discrimination through differential whisker resonances.

## Conflict of interest statement

The authors do not have any conflicts of interest.

## Appendix A. Supporting information

Supplementary data associated with this article can be found in the online version at <http://dx.doi.org/10.1016/j.jbiomech.2013.06.015>.

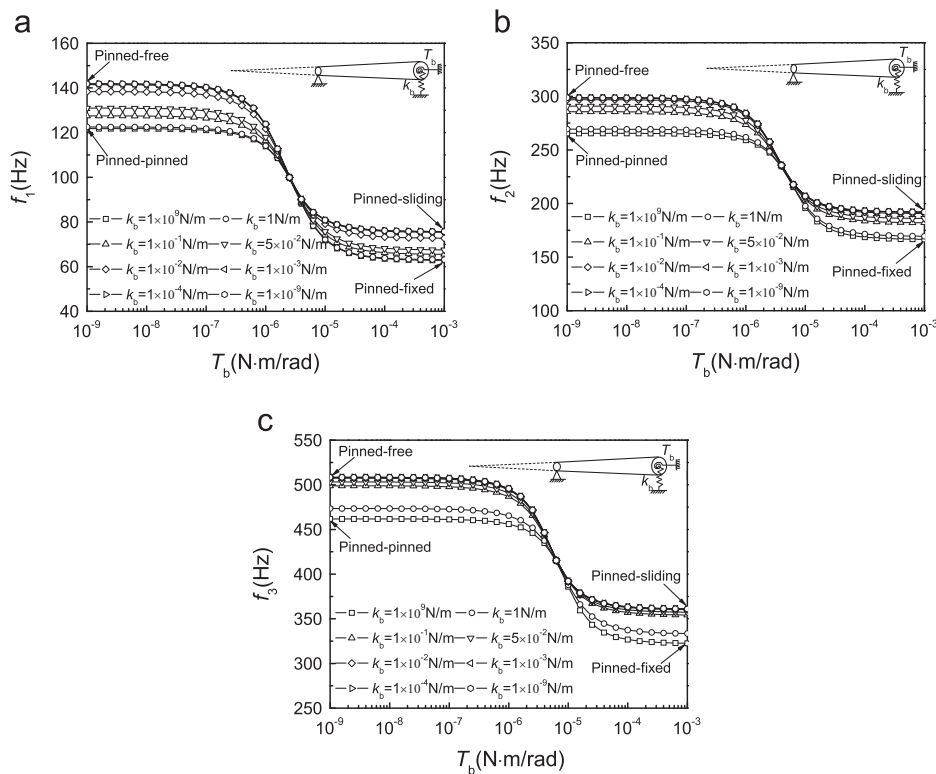


**Fig. 6.** The natural frequencies of a representative rat whisker with the tip touching an object under different elastic constraining stiffnesses  $k_b$  and  $T_b$  at the base: (a) the first natural frequency; (b) the second natural frequency; and (c) the third natural frequency.

## References

- Andermann, M.L., Moore, C.I., 2008. Mechanical resonance enhances the sensitivity of the vibrissa sensory system to near-threshold stimuli. *Brain Research* 1235, 74–81.
- Andermann, M.L., Ritt, J., Neimark, M.A., Moore, C.I., 2004. Neural correlates of vibrissa resonance: band-pass and somatotopic representation of high frequency stimuli. *Neuron* 42, 451–463.
- Birdwell, J.A., Solomon, J.H., Thajchayapong, M., Taylor, M.A., Cheely, M., Towal, R.B., Conradt, J., Hartmann, M.Z., 2007. Biomechanical models for radial distance determination by the rat vibrissal system. *Journal of Neurophysiology* 98, 2439–2455.
- Buckingham, E., 1914. On physically similar systems; illustrations of the use of dimensional equations. *Physics Review* 4, 345–376.
- Carl, K., Hild, W., Mämpel, J., Schilling, C., Uhlig, R., Witte, H., 2012. Characterization of static properties of rat's whisker system. *IEEE Sensors Journal* 12, 340–349.
- Carvell, G.E., Simons, D.J., 1990. Biometric analyses of vibrissal tactile discrimination in the rat. *Journal of Neuroscience* 10, 2638–2648.
- Conway, H.D., Becker, E.C.H., Dobil, J.F., 1964. Vibration frequencies of tapered bars and circular plates. *Journal of Applied Mechanics* 31, 329–331.
- Conway, H.D., Dobil, J.F., 1965. Vibration frequencies of truncated cones and wedge beams. *Journal of Applied Mechanics* 32, 932–934.
- Ebara, S., Kumamoto, K., Matsuura, T., Mazurkiewicz, J.E., Rice, F.L., 2002. Similarities and differences in the innervation of mystacial vibrissal follicle–sinus complexes in the rat and cat: a confocal microscopic study. *Journal of Comparative Neurology* 449, 103–119.
- Georgian, J., 1965. Vibration frequencies of tapered bars and circular plates. *Journal of Applied Mechanics* 32, 234–235.
- Hartmann, M.J., Johnson, N.J., Towal, R.B., Assad, C., 2003. Mechanical characteristics of rat vibrissae: resonant frequencies and damping in isolated whiskers and in the awake behaving animal. *Journal of Neuroscience* 23, 6510–6519.
- Herzog, E.K., Bahr, D.F., Richards, C.D., Richards, R.F., Rector, D.M., 2005. Spatially dependent mechanical properties of rat whiskers for tactile sensing. *Materials Research Society Symposium Proceedings* 841, R3.6.1–R3.6.5.
- Jadhav, S.P., Feldman, D.E., 2010. Texture coding in the whisker system. *Current Opinion in Neurobiology* 20, 313–318.
- Krupa, D.J., Matell, M.S., Brisben, A.J., Oliveira, L.M., Nicolelis, M.A.L., 2001. Behavioral properties of the trigeminal somatosensory system in rats performing whisker-dependent tactile discriminations. *Journal of Neuroscience* 21, 5752–5763.
- Moore, C.I., 2004. Frequency-dependent processing in the vibrissae sensory system. *Journal of Neurophysiology* 91, 2390–2399.
- Moore, C.I., Andermann, M.L., 2005. The vibrissa resonance hypothesis. In: Ebner, F.F. (Ed.), *Neural Plasticity in Adult Somatic Sensory-Motor Systems*. Taylor & Francis Publishing Group, CRC Press, Boca Raton, FL, pp. 21–59.
- Neimark, M.A., Andermann, M.L., Hopfield, J.J., Moore, C.I., 2003. Vibrissa resonance as a transduction mechanism for tactile encoding. *Journal of Neuroscience* 23, 6499–6509.
- Quist, B.W., Faruqi, R.A., Hartmann, M.Z., 2011. Variation in Young's modulus along the length of a rat vibrissa. *Journal of Biomechanics* 44, 2775–2781.
- Rice, F.L., Fundin, B.T., Arvidsson, J., Aldskogius, H., Johansson, O., 1997. Comprehensive immunofluorescence and lectin binding analysis of vibrissal follicle sinus complex innervation in the mystacial pad of the rat. *Journal of Comparative Neurology* 385, 149–184.
- Ritt, J.T., Andermann, M.L., Moore, C.I., 2008. Embodied information processing: vibrissa mechanics and texture features shape micromotions in actively sensing rats. *Neuron* 57, 599–613.
- Sanger, D.J., 1967. Transverse vibration of a class of non-uniform beams. *Journal of Mechanical Engineering Science* 10, 111–120.
- Szwed, M., Bagdasarian, K., 2003. Encoding of vibrissal active touch. *Neuron* 40, 621–630.
- Voges, D., Carl, K., Klauer, G., Uhlig, R., Schilling, C., Behn, C., Witte, H., 2010. Structural characterisation of the whisker system of the rat. *Sensors*, 4718.
- Weaver Jr., W., Timoshenko, S., Young, D.H., 1990. *Vibration Problems in Engineering*, fifth ed. John Wiley & Sons, Inc, New York.
- Wolfe, J., Hill, D.N., Pahlavan, S., Drew, P.J., Kleinfeld, D., Feldman, D.E., 2008. Texture coding in the rat whisker system: slip-stick versus differential resonance. *PLoS Biology* 6 (e215), 1661–1677.